Peer-reviewed version available at J. Funct. Biomater. 2019; doi:10.3390/jfb10040052

Article

Growth and differentiation of human Wharton's jelly mesenchymal stem cells on oxygen plasma-modified 2D and 3D polycaprolactone scaffolds

Kewalin Inthanon [1], Weerah Wongkham [2], Wanida Junwikul [3] and Siriwadee Chomdej [2, 4,*]

[1] Department of Biotechnology, Faculty of Science and Technology, Thammasart University, Lampang, 52190, Thailand; kelly_inthanon@hotmail.com
[2] The Human and Animal Cell Technology Research Unit. Department of Biology, Faculty of Science, Chiang Mai University, Chiang Mai, 50200, Thailand; wwongkham@gmail.com
[3] National Metal and Materials Technology Center, Pathumthani 12120, Thailand; wanida@mtec.or.th
[4] Center of Excellence in Bioresources for Agriculture, Industry and Medicine Chiang Mai University
* Correspondence: siriwadee@yahoo.com; Tel.: +66-869-143-228

Abstract: Cell-based therapies and tissue engineering applications require biocompatible substrates that support and regulate the growth, survival, and differentiation of specific cell types. Extensive research efforts in regenerative medicine are devoted to the development of tunable biomaterials which support various cell types including stem cells. In this research, the non-cytotoxic biopolymer polycaprolactone (PCL) was fabricated into 2D and 3D scaffolds with or without the low-pressure oxygen plasma treatment to enhance hydrophilicity. Cellular responses and biocompatibility were evaluated using a human Wharton's jelly mesenchymal stem cell line (BCP-K1). The 2D PCL scaffolds enhanced initial cell attachment compared to the 3Ds indicated by a higher expression of focal adhesion kinase (FAK). Whilst, the 3D scaffolds promoted cell proliferation and migration as evidenced by higher cyclin A expression and filopodial protrusion, respectively. The 3D scaffolds potentially protected the cell entering to apoptosis/necrosis program and induced cell differentiation, evaluated by gene expression. Both 2D and 3D PCL appeared to have stronger effects on cell behavior than a control substrate (polystyrene). In summarize, the different configuration and surface properties of PCL scaffolds provide various options for modulation of stem cell behaviors, including attachment, proliferation, survival, and differentiation, when combined with specific growth factors and culture conditions.

Keywords: polycaprolactone; oxygen plasma; Wharton's Jelly mesenchymal stem cells

1. Introduction

Improved substrate material biocompatibility for regenerative medicine has been the focus of intensive research efforts for several decades [1]. Material composition and fabrication technique must be carefully selected according to target cell type and ultimate application. The surface architecture of these materials has been refined to micro- and nanoscales in order to mimic specific cell niches. In cell-based therapy, the biomaterial must permit cell attachment, proliferation, homeostasis, and tissue formation [2-4]. However, many limitations of previous biomaterial support platforms have been encountered, including an inability to control cell growth and differentiation [5]. In addition, most regenerative medicine and tissue engineering techniques are based on exogenous cell-culture systems that may induce graft-versus host disease. In response, endogenous regenerative medicine has been developed in which the patient's own cells or tissues are used [6] to support and promote cell proliferation, survival, and differentiation, thereby increasing intrinsic regenerative capacity after transplantation [7]. Not all biomaterials can support all cell types, including stem cells.

Hence, establishing a tunable material may facilitate a new generation of multidisciplinary regenerative medicine applications.

Polycaprolactone (PCL) is a polymer with known biocompatibility. Moreover, treatment of PCL with oxygen plasma increases hydrophilicity and induces chemical surface remodeling without altering the basic topography [8], properties that can significantly enhance cell attachment and proliferation [4]. Substrate geometry is also an important determinate of stem cell behavior on PLC and other materials. For instance, 2D scaffolds are generally considered more suitable for tissue layer construction such as skin and cornea, while 3D scaffolds may be more applicable for complex tissue formation by permitting the coordinated cell–cell and cell–matrix interactions required for appropriate cell migration and differentiation [9].

The current study aimed to develop and evaluate a tunable biomaterial with the potential for stem cell modulation and ERM applications. Non-cytotoxic biodegradable PCL was fabricated by a high pressure super critical CO2 technique followed by low pressure oxygen plasma surface modification as described by Kosorn et al. (2012) [10]. PCL scaffolds were constructed as 2D and 3D platforms and assessed for biocompatibility by evaluating attachment, proliferation, apoptosis, stemness maintenance, and differentiation of the human Wharton's jelly mesenchymal stem cell (hWJMSC) line BCP-K1. The introduction should be succinct, with no subheadings. Limited figures may be included only if they are truly introductory, and contain no new results.

2. Materials and Methods

2.1 Standard Cell Culture

The hWJMSC line BCP-K1 was obtained from The Human and Animal Cell Culture Research Unit, Department of Biology, Faculty of Science, Chiang Mai University, Thailand. Cells were maintained and propagated in a complete medium containing Dulbecco's Modified Eagle Medium (DMEM) supplemented with 10% (v/v) fetal bovine serum (FBS) and 2 ng/ml basic fibroblast growth factor (bFGF) (all from Gibco, USA). Cells were incubated at 37°C under an atmosphere with 95% humidity and 5% CO2. The medium was replaced every 2-3 days. At 70% confluence, cells were subcultured by trypsinization.

2.2 Preparation of Plasma Modified 2D and 3D PCL Scaffolds

Scaffolds of PCL in 2- and 3-dimensional (2D and 3D) forms were obtained from National Metal and Materials Technology (MTEC, Bangkok, Thailand). Fabrication and oxygen plasma surface modification were performed as previously described by Kosorn et al. (2012) [10]. Briefly, the 2D PCL scaffolds were prepared by hydrolysis of PCL pellets (Sigma Aldrich, USA) in 6 N NaOH at 50°C for 5 h, followed by soaking in deionized water and freeze-drying overnight. For 3D scaffold preparation, PCL pellets were loaded into a cylindrical vessel, heated at 60°C for 10 min, filled with CO2 at 15 MPa, and then soaked in deionized water for 3 h. Both 2D and 3D PCL scaffolds were then treated with pure oxygen plasma using a low-pressure radiofrequency discharge plasma cleaner (model PDC-002, Harrick) at 30 W for 30 min. In this study, plasma-treated 2D and 3D PCL scaffolds are abbreviated as 2D-TP and 3D-TP, while untreated 2D and 3D PCL scaffolds are termed 2D-NP and 3D-NP, respectively. All types of scaffolds were finely cut into small circular pieces 0.6 cm in diameter. To sterilize the scaffolds for cell culture, each side was exposed for 15 min to standard UV light in a biosafety cabinet. Sterile circular pieces were then placed into 96-well plates filled with complete medium and seeded as described. These "ready-to-use scaffolds" were prepared at least 30 min prior to cell culture experiments.

2.3 Cell Proliferation and Attachment Assays

The BCP-K1 cells were suspended at 3×10^5 cell/ml in medium and seeded onto the PCL scaffolds or polystyrene (PS) as a control and maintained for 1, 3, or 5 days in culture as described, followed by analyses of cell proliferation and attachment by enzyme-linked immunosorbent assay (ELISA). Focal adhesion kinase (FAK) and cyclin-A protein expression levels were used as markers for cell

Peer-reviewed version available at J. Funct. Biomater. 2019; doi:10.3390/jfb10040052

proliferation and attachment, respectively. The assays were performed as described by Inthanon et al. (2016) [11]. Briefly, cells were fixed in 4% (v/v) formaldehyde for 30 min at room temperature and then washed three times (5 min/wash) with ice-cold washing buffer (0.05% (v/v) Tween 20 in 1X PBS) with gentle rocking. The samples were subsequently immersed in quenching buffer containing 1X PBS, 1% (v/v) H2O2, and 0.1% (v/v) sodium azide for 20 min and then in blocking solution containing 5% (v/v) bovine serum albumin (BSA) for 1 h. Diluted anti-FAK and anti-cyclin-A primary antibodies were added drop-wised onto the samples and incubated at 4°C overnight. A horseradish peroxidase (HRP)-labeled secondary antibody was added onto each sample for 1 h before applying the HPR substrate, o-phenylenediamine dihydrochloride (OPD) (all purchased from Sigma-Aldrich). The absorbance was read at 492 nm on a microplate reader. Five independent replicates were performed for each sample.

2.4 Observation of Cellular Attachment under Scanning Electron Microscopy (SEM)

Attached cells were fixed in 2.5% (w/v) glutaraldehyde (Sigma-Aldrich, USA) for 20 min after 1, 4, 12, 24, or 72 h in culture. The samples were washed three times with PBS (5 min per wash) with gentle rocking, dehydrated in graded ethanol solutions, and then air-dried at room temperature. The samples were set onto copper stubs and coated with gold particles in a sputter unit (SPITM Module Sputter/Carbon Coater system, SPI® supplies, USA). Cell morphology on both 2D and 3D PCL scaffolds was observed under SEM.

2.5 Gene Expression by Semi-Quantitative Polymerase Chain Reaction (PCR)

A 3×10^5 cell/ml suspension of BCP-K1 cells was seeded on 2D PLC scaffolds, 3D PCL scaffolds, or PS and then maintained in culture for 5 days prior to RNA extraction. In this experiment, the PS control was divided into two subsets; 1-day and 5-day culture which are abbreviated as 1d-ctrl and 5d-ctrl, respectively. Total RNA extraction and first strand cDNA synthesis were performed by using RNA extraction kit (NucleoSpin® RNAII, Fisher Scientific, Ireland). First strand cDNA was synthesized from mRNA via reverse transcriptase reaction using a Phusion® RT-PCR kit (Thermo Scientific, USA). The cDNA solution was read the absorbance at 280 nm by using NanoDrop®1000 (Thermo Scientific, USA). The absorbance values were then calculated to total cDNA concentrations. The cDNA (100 ng per sample) was used as the template for gene expression assessment by semi-quantitative PCR. Two gene groups were examined: (i) the apoptosis/necrosis-related genes *caspase 8*, *Apaf-1*, *Bcl-2*, and *PARP-1* and (ii) the pluripotency/differentiation-related genes *SSEA-4*, *NES* (encoding *nestin*), *COL2A1*, and *PPAR-2*. *GAPDH* was used as the internal control for all reactions. The primer sequences (with accession numbers) for each gene are shown in Table 1. PCR products were electrophoresed on 1% (w/v) agarose gels at 75 V for 45 min and bands photographed under a UV-transilluminator. Gene expression was indirectly quantified as band intensity using ImageJ software (NIH). Expression levels were normalized to *GAPDH* expression and then 1d-ctrl. Each experimental condition was repeated five times.

2.6 Statistical Analysis

All data are presented as mean ± standard deviation (SD). Treatment group means were compared by student's T-test and ANOVA for independent or paired samples, respectively. A P value ≤ 0.05 was considered statistically significant for all tests.

Table 1. Primer sequences and accession numbers

Gene	Accession number	Sequence
caspase 8	NM_001228.4	F: 5'-TGCAGGGGCTTTGACCACGA-3' R: 5'-TGGGGGCCTCCTGTCCATCA-3'
bcl-2	NM_000633.2	F: 5'-TGTGGCCTTCTTTGAGTTCG-3' R: 5'-TCACTTGTGGCTCAGATAGG-3'
Apaf-1	NM_013229.2	F: 5'-TGGCCAGTGCCAAGATGCACA-3' R: 5'- CGACCTCCTGCTTGGCCTGC-3'
PARP-1	NM_017915.3	F: 5'-AATCTCCAGGGGGTAGAACT-3' R: 5'-CAGAGCCTGTTGAAGTTGTG-3'
SSEA-4	NM_203289.4	F: 5'-GCCCTAGAACTCCAATCACA-3' R: 5'-CCCAGATGGTATTGGACACA-3'
NES	NM_006617.1	F: 5'-TCCTGCTCGCTCTCTACTTT-3' R: 5'-CCCAGATGGTATTGGACACA-3'
COL2A1	NM_001844.4	F: 5'-CCCATTGGTCCTTGCATTAC-3' R: 5'-GTCCTCTGCGACGACATAAT-3'
PPAR-2	NM_138712.3	F: 5'-GCATTATGAGACATCCCCACT-3' R: 5'-CCTATTGACCCAGAAAGCGAT-3'
GAPDH	NM_002046.4	F: 5'-TGCTGGCGCTGAGTACGTCG-3' R: 5'-TGACCTTGGCCAGGGGTGCT-3'

3. Results

3.1. Differences in Cell Attachment and Proliferation Between Cells Growing on 2D and 3D Scaffolds

The capacities of PLC scaffolds to support attachment and proliferation of BCP-K1 cells were evaluated by ELISA of FAK and cyclin-A protein expression, respectively. ELISA results showed that BCP-K1 cultures expressed higher FAK levels on 2D PCL scaffolds (both 2D-TP and 2D-NP) than on 3D scaffolds on all test days (Figure 1a). The time course of the expression changes also differed among substrates. On 2D-TP and 2D-NP scaffolds, FAK expression increased progressively with time, while FAK expression decreased with time on 3D-TP and 3D-NP scaffolds. Further, expression on 3D-TP scaffolds was markedly lower than on control PS and untreated 2D-TP scaffolds on all days. Conversely, cyclin-A expression on day 1 was substantially lower in cells growing on 2D-TP, 2D-NP, and control scaffolds than on 3D-TP and 3D-NP scaffolds. However, expression on 2D and control scaffolds increased progressively while expression on 3D scaffolds peaked on day 3 and decreased markedly thereafter (Figure 1b). This expression pattern indicates high cell proliferation rate on the limited surface area of the 3D scaffolds until day 3, at each time cells reached confluence and cyclin-A is downregulated concomitant with proliferation rate (Figure 1b).

3.2 Cellular Attachment on Different Substrates

The morphology of BCP-K1 cells was monitored by SEM during culture for 72 h on the indicated substrate (Figure 2). These SEM pictures revealed a faster rate of cell attachment on 2D scaffolds as evidenced by a generally flattener spindle shape and greater numbers of foot adherent pads (filopodia) compared to cells on other substrates (Figure 2, 3). Alternatively, cells on 3D scaffolds remained spherical for up to 4 h before attaching onto the surface and primarily exhibited irregular

Peer-reviewed version available at J. Funct. Biomater. 2019; doi:10.3390/jfb10040052

shapes and large adherent patches of cytoplasm around the nucleus (Figure 2a and 2b on 3D-TP and 3D-NP column). In addition, cells growing on 2D PLC scaffolds exhibited more numerous filopodial structures (Figure 3a, 3b). Cells on 3D-NP scaffolds tended to migrate more readily than cells on 3D-TP scaffolds as evidenced by the greater number of filopodial protrusion (Figure 3d, 3e). However, more cells on 3D scaffolds exhibited irregular shapes and undefined cytoplasmic edges compared to cells on 2D PCL scaffolds.

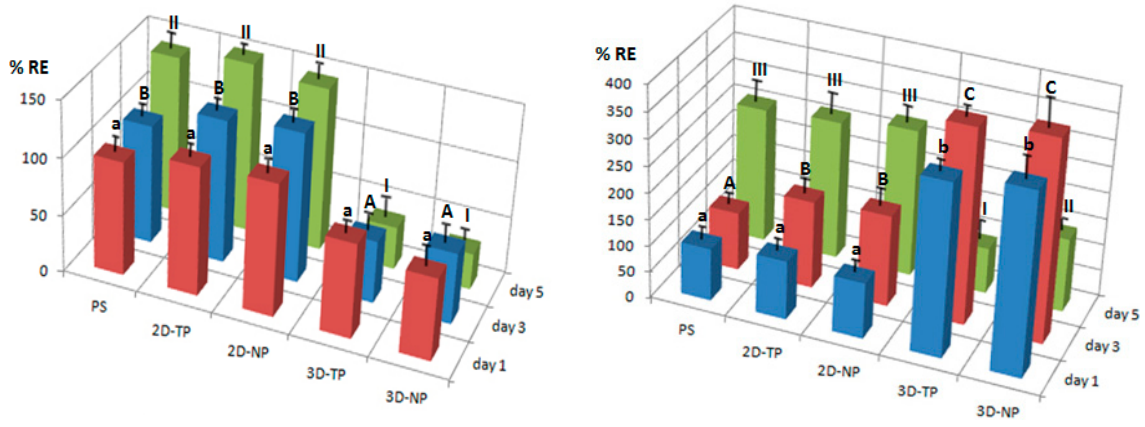

(**a**) (**b**)

Figure 1. Relative percent expression (%RE) of (**a**) FAK and (**b**) cyclin-A protein by BCP-K1 cells cultured on different scaffold types for 1, 3, and 5 days as evaluated by ELISA. The letters and Roman numerals on top of the bars represent significant differences ($p \leq 0.05$) in expression compared to day 1 (a, b), day 3 (A, B, C), and day 5 (I, II, III).

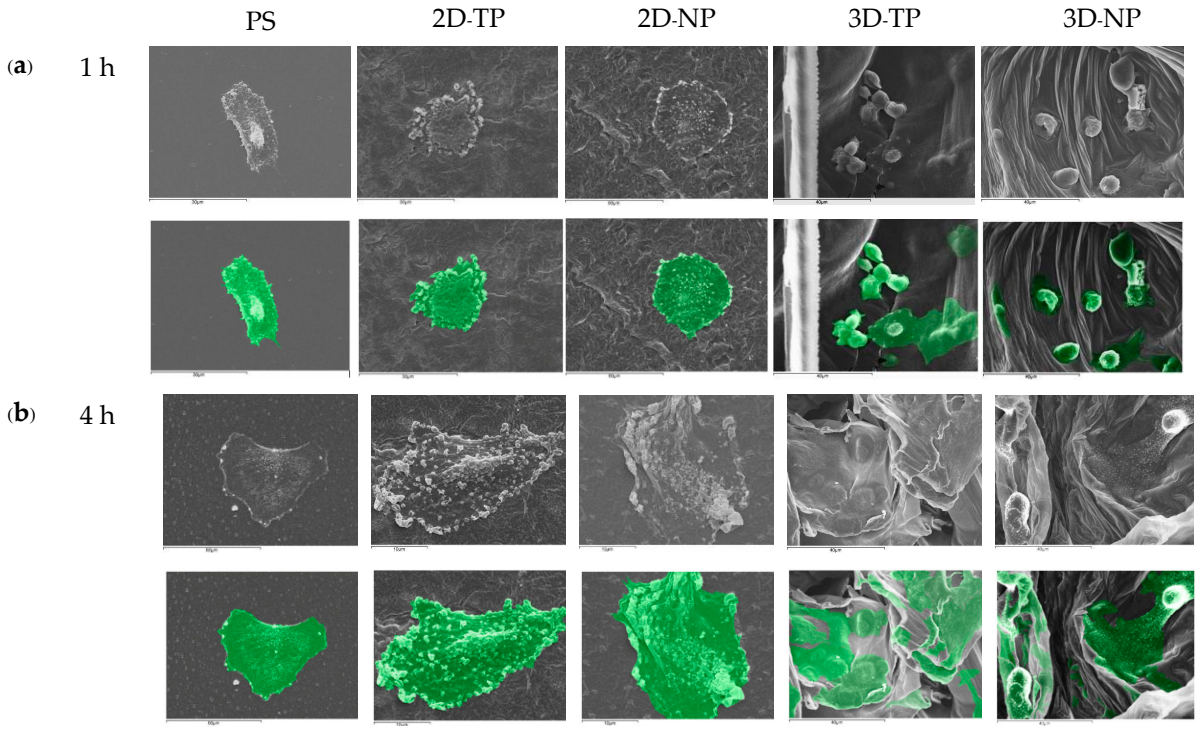

Peer-reviewed version available at J. Funct. Biomater. 2019; doi:10.3390/jfb10040052

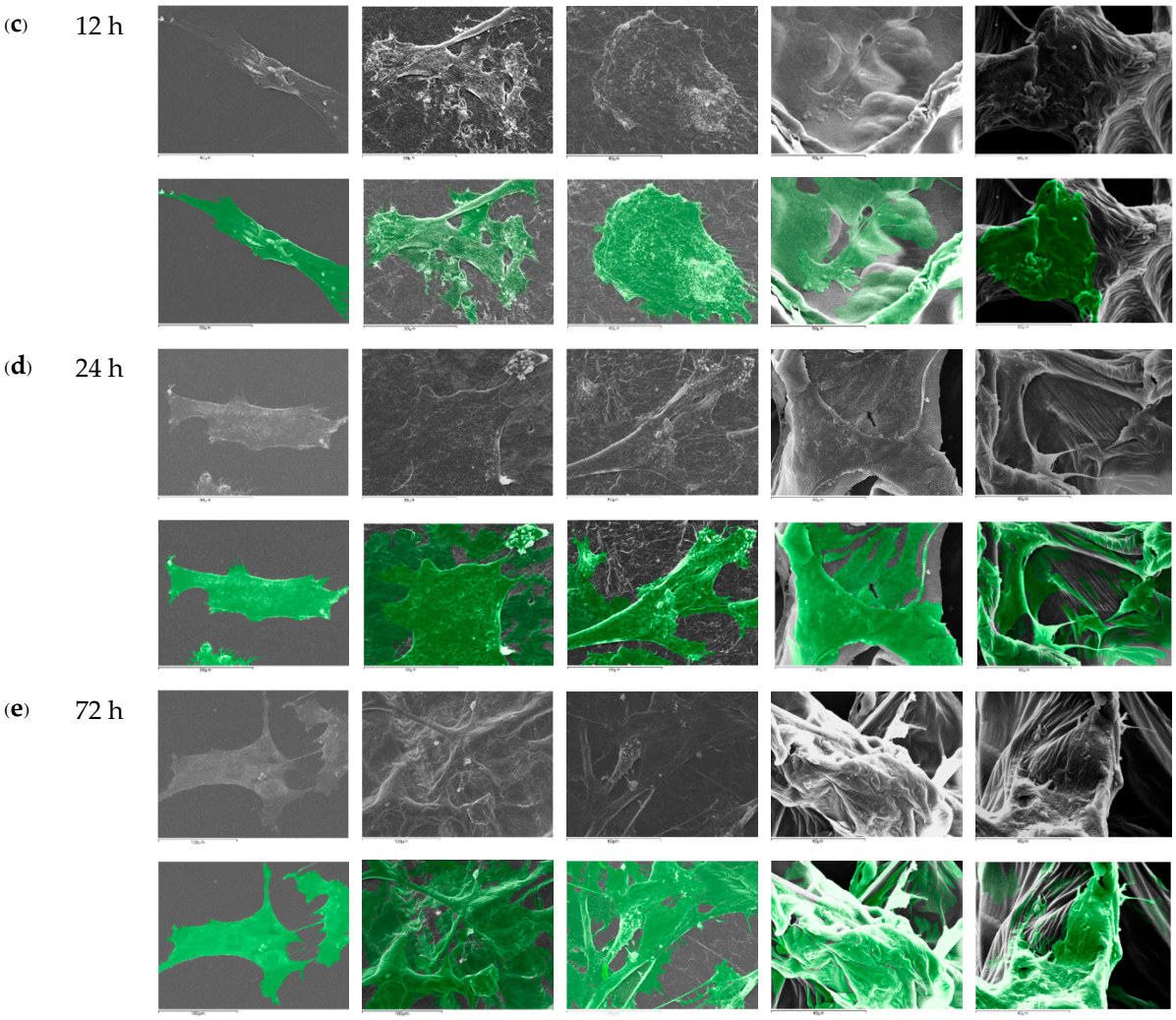

Figure 2. SEM pictures of BCP-K1 morphology on PS, 2D-TP, 2D-NP, 3D-TP and 3D-NP PCL scaffolds at various time of culture (1-72 h) (magnification = 1,000X). The second row of each time point indicates the cell boundary and position on the scaffolds (exhibiting in green).

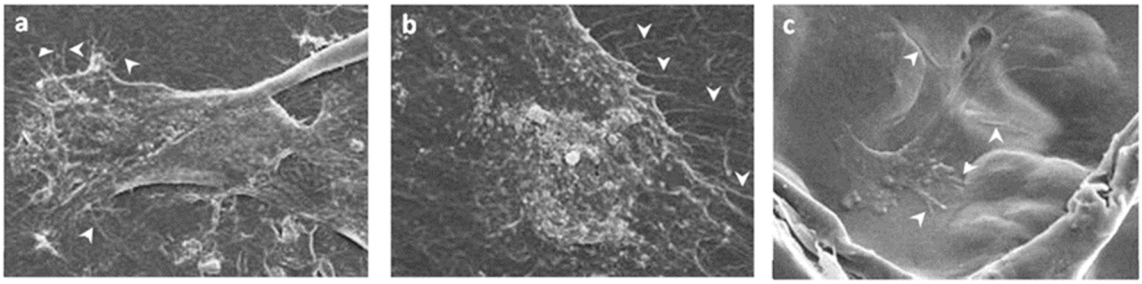

(**a**) (**b**) (**c**)

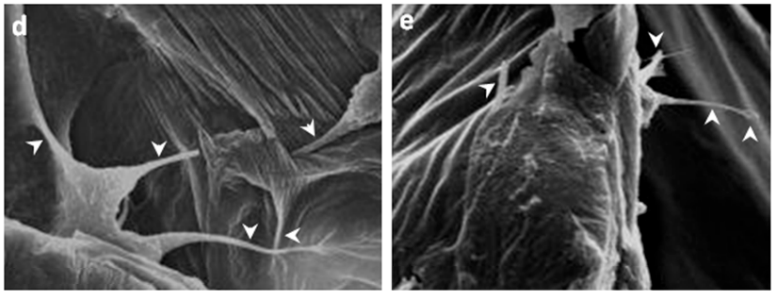

(**d**) (**e**)

Figure 3. Filopodial protrusions (white arrows) around the cytoplasmic edge at 12 h of culture on (a) 2D-TP (b) 2D-NP, and (c) 3D-TP scaffolds. Cells on 3D-NP scaffolds extended more numerous filopodia than cells on 3D-TP scaffolds at (d) 24 h and (e) 72 h (magnification = 4,300X).

3.3 Shifts in Apoptosis/Necrosis-related and Pluripotency/Differentiation-related Gene Expression on Different Substrates

3.3.1. Apoptosis/Necrosis-related Genes

To evaluate whether the scaffolds could support cell survival, the expression levels of multiple apoptosis/necrosis-related genes were investigated by RT-PCR. The apoptotic-related genes caspase 8 and *bcl-2* were detectable in all cultures (Figure 4). Co-expression of *caspase 8*, *Apaf-1*. and *PARP-1* was found in 1d-ctrl and other 5d-ctrl (Figure 4, 5a). On 2D-PCL scaffolds, pro-apoptotic *caspase 8* expression was higher than anti-apoptotic *bcl-2* expression, while cultures on 3D-PCL scaffolds expressed slightly more *bcl-2* than *caspase 8* (Figure 4, 5a).

3.3.2. Pluripotency/Differentiation-related Genes

The pluripotency/differentiation status of cells cultured on each type of substrate was also evaluated. The highest expression of the stem cell marker SSEA-4 was observed in control cells and the lowest level in cells growing on 3D-TP scaffolds. The rank order of expression was 5d-ctrl^{c} = 2D-TP^{c} ≥ 2D-NP^{bc} ≥ 3D-NP^{b} (Figure 4, 5b). The control cultures also exhibited the highest expression level of the neural progenitor marker NES. Overall rank order was 5d-ctrl^{B} = 2D-NP^{B} > 2D-TP^{AB} = 3D-NP^{AB} and 3D-TP^{A} (Figure 4, 5b). Expression levels of the chondrocyte marker *COL2A1* and adipocyte marker *PPAR-2* were undetectable in all cultures (data not shown).

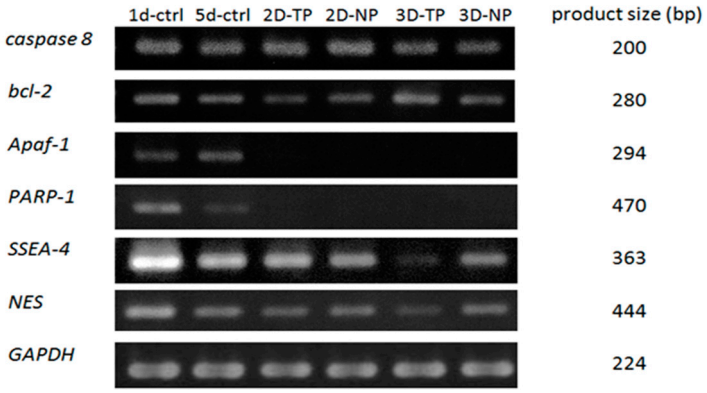

Figure 4. PCR products were electrophoresed on agarose gels. Band intensity was used as a semi-quantitative measure of gene expression level after 5 days in culture. The PCR product size of each gene is shown in the right column.

Peer-reviewed version available at J. Funct. Biomater. 2019; doi:10.3390/jfb10040052

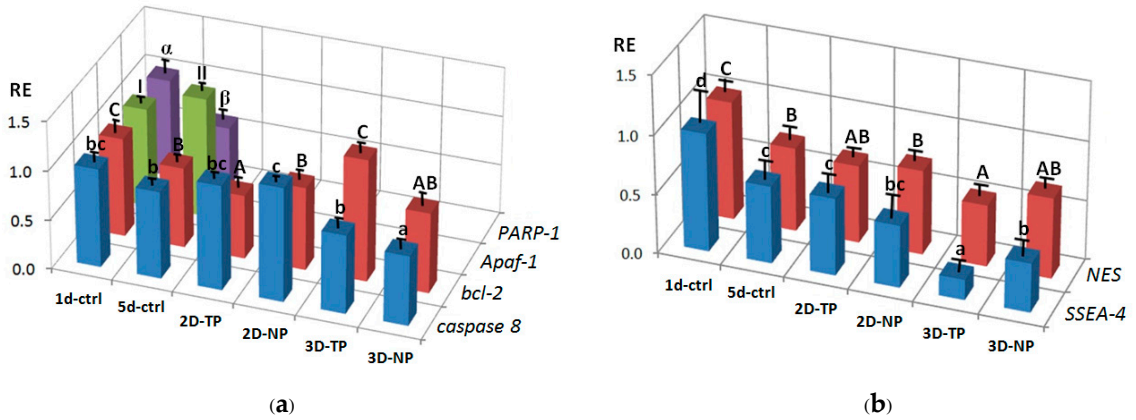

(**a**) (**b**)

Figure 5. Relative expression (RE) levels of (a) apoptosis/necrosis-related genes and (b) pluripotency/differentiation-related genes. The letters, Roman numerals, and Greek symbols on top of the bars represent significant differences ($p \leq 0.05$) of relative gene expression in (a) a-c for *caspase-8*, A-C for *bcl-2*, I-II for *Apaf-1*, and α-β for *PARP-1* and in (b) a-c for *SSEA-4* and A-B for *NES*) on the indicated substrate.

4. Discussion

Polycaprolactone synthetic polymer was introduced more than a decade ago and has since been used extensively as a biomaterial for tissue engineering and regenerative medicine due to advantageous properties such as non-cytotoxicity and tunable biodegradability [1,12]. Moreover, many laboratories worldwide have continued to improve the biocompatibility of PCL, for instance by increasing its hydrophilicity [2-4]. Oxygen plasma surface modification has been reported to increase the hydrophilicity of PCL polymer, resulting in better cell attachment and proliferation [1, 4, 13]. In addition to surface properties, the geometric form (2D or 3D) of the biopolymer has a substantial influence on proliferation, differentiation, and survival [14, 15]. In this study, we found substantial differences in proliferation, differentiation, and survival of the hWJMSC line BCP-K1 depending on substrate (PS or PCL), conformation (2D or 3D), and surface hydrophilicity (oxygen plasma-treated and untreated). These results suggest that PLC is a flexible substrate for multiple applications in regenerative medicine and tissue engineering.

Substrate attachment of anchorage-dependent cells is crucial for subsequent morphological development, proliferation, and differentiation [16]. In this study, the attachment and proliferation efficiencies of BCP-K1 cells on PCL scaffolds were evaluated by the expression of FAK and cyclin-A, respectively. The non-receptor tyrosine kinase FAK is strictly required for cell–extracellular matrix (ECM) interactions during substrate adhesion [17]. The survival and proliferation of anchorage-dependent cells requires FAK as a responsive mediator of integrin signaling [18, 19]. FAK and other associated signaling pathways were demonstrated to regulate the cell cycle via cyclins and cyclin-dependent kinases (Cdks) [19-21]. Cyclin-A was chosen as a protein marker for cell proliferation capacity in the current study as it is a vital component of the cell cycle machinery [22, 23]. FAK expression was significantly higher in cells on 2D scaffolds. A rougher surface on 2D scaffolds may enhance cell attachment and proliferation compared to 3D scaffolds due to significantly greater FAK expression and phosphorylation [24-26]. Alternatively, the pores on 3D scaffolds may act as spatially limiting compartments influencing the concentrations of various signaling ligands, resulting in lower FAK expression [19]. However, in a stressful environment after initial seeding (such as growth on the stiffer ECM under lower ligand stimulation), alternative signaling via RhoA protein to control the cell cycle through regulation of cyclin proteins may occur [21, 27, 28]. This difference may explain why higher levels of cyclin-A were found during the early days after seeding on 3D PCL scaffolds.

Despite the difference in surface hydrophilicity between plasma-treated and untreated surfaces (approximately 3-fold [10]), there were no substantial differences in FAK and cyclin-A expression levels between TP and NP substrates. However, degradation rate of the material also increases after treatment, leading to rapid loss of functional groups and other essential active molecules from the

surface [29]. Preparation of material by washing and soaking in ethanol and PBS may have also enhanced surface degradation, resulting in losing oxygen plasma and other functional molecules on the surface, mitigating any potential difference in FAK and cyclin-A expression among PS, TP, and NP substrates.

The biocompatibility of PCL for cell−cell and cell−matrix interactions has been confirmed [30, 31]. The surface microtopography of materials directly influences attachment patterns, cell shape, and spread [32, 33]. According to SEM, 2D scaffolds appeared to accelerate the initial rate of cell attachment. It is speculated that the surface of the 2D scaffolds provided anchorage points for initial attachment to hold the cell body in place, allowing subsequent filopodial protrusion to regulate cell shape and further growth [34]. Indeed, more numerous filopodial structures on 2D PCL scaffolds has been shown to promote greater cell attachment [35, 36]. This result was further verified by the increased FAK expression described here, as filopodial shafts contain signaling pathways (e.g. FAK, Rac1/Cdc42/RhoA) promoting substrate adhesion [37]. Some studies have revealed that in 3D environments, cells generally migrate into the substrate by producing various protrusion types, including some large adhesion patches called lamellipodia [38]. In fact, newly seeded cells transiently may express filopodia for early attachment, which quickly disappear [39] or are converted into lamellipodia [You et al., 2014]. When migrating cells reach new environments, filopodia protrusion is initiated to detect surface topography, as observed on 3D-NP scaffolds (Figure 3d, 3e). These protrusions are then converted into lamellipodia and direct cell shape and spread [40, 41]. Fewer filopodial protrusions and the conversion to lamellipodia may have conferred the irregular cell shape and undefined cytoplasmic edges observed in 3D PCL scaffold culture.

Cytotoxicity and viability testing are essential for biomaterial development but provide insufficient information for actual medical applications. In addition, other biological properties of the scaffolds have to be addressed in order to understand how they affect the target cells. Some scaffolds offer proper surface topography for cell adherence, but not proliferation, which leads to cell death [42, 43]. There are 2 major types of cell death, apoptosis and necrosis, each governed by distinct regulatory mechanisms and having unique biological and morphological manifestations [44]. Apoptosis or programmed cell death (PCD) is a key mechanism for embryogenesis and homeostasis in multi-cellular organisms. In contrast, spontaneous necrosis or cell lysis is a cellular response to acute non-physiological injuries [45]. Initiation of either programmed apoptosis or necrosis is induced by external stimuli through a death ligand that subsequently activates a signaling cascade including caspase family proteins. Programmed death appears to follow 3 routes; (1) *caspase 8* activation by external death signals cleaves an effector caspase (such as *caspase 3*) leading to apoptosis through an extrinsic pathway [46], or (2) mitochondria-mediated release of cytochrome C initiates apoptosome formation via the apoptotic protease activating factor, *Apaf-1*, activating the intrinsic apoptotic pathway [47, 48], and (3) external death signals stimulate *PARP-1*, resulting in programmed necrosis distinct from caspase-independent PCD [45, 49]

Whether cells survive or die under specific conditions is determined by the balance between expression levels of competing gene groups involved in cell fate decisions [50]. The expression of caspase 8 was detectable in all culture samples, but this does not necessarily indicate apoptosis without co-expression of other downstream pro-apoptotic factors (e.g., *Apaf-1* or *PARP-1*). Co-expression of *caspase 8*, *Apaf-1*, and *PARP-1* was found in 1d-ctrl and 5d-ctrl, suggesting that some cells were undergoing apoptosis via an intrinsic pathway and/or necrosis pathway via activated *caspase 8*/*Apaf-1* [47,48] and *PARP-1*, respectively [45, 49]. On 2D PCL scaffold cultures, *caspase 8* expression was higher than *bcl-2* expression, suggesting activation of an extrinsic apoptosis pathway, while cultures on 3D PCL scaffolds expressed slightly more *bcl-2* than caspase 8, suggesting that most cells were able to grow and survive due to the anti-apoptotic actions of *bcl-2* [51].

Numerous specific combinations of stem cells and biomaterials have been examined to improve the intrinsic properties of scaffolds and understand how they influence proliferation and differentiation [52-54] in this study. *SSEA-4* was chosen as a marker for stem cell self-renewal [55], while *NES*, *COL2A1*, and *PPAR-2* genes were used to assess differentiation to neural, chondrocyte, and adipocyte lineages [55]. Co-expression of pluripotency and differentiation markers (*SSEA-4* and

NES) observed in control cultures may result from the specific culture conditions employed. The presence of bFGF in the culture medium can induce *NES* expression (as well as the expression of other neural markers) without changing cell morphology [55-57]. *SSEA-4*-positive MSCs can be induced to either neural or non-neural lineages [55]. Alternatively, the cells may be in an intermediate state between multipotent and differentiated [55, 58]. In addition, differentiation capacity of cells is limited by density. A high density of WJMSCs at confluence reduces proliferation rate, decreases colony-forming capacity, and ultimately leads to loss of multipotency [59] (pp. 45–72). Hence, 1d-ctrl and 5d-ctrl were enriched in bFGF at low cell density, and so expressed highest levels of *SSEA-4* and *NES*. With time in culture and concomitant proliferation, cells may have consumed most bFGF from the medium. Thus, by the time cells reached confluence on day 5, there was a decrease in *SSEA-4* and NES expression in all samples. The lowest levels of *SSEA-4* and *NES* expression were observed in cells on 3D-TP PCL scaffolds, suggesting that these cells may reach confluence before day 5, resulting in loss of proliferation capacity and/or self-renewal (stemness). Further, the 3D structure provides physical guidance supporting cell attachment and spread, thereby promoting more rapid proliferation [61] during the early period after seeding. Interestingly, long-term culture of MSCs in medium supplemented with bFGF induced loss of osteogenic/adipogenic differentiation potential [59] (pp. 45–72), while adding bFGF to a chondrocyte precursor culture inhibited chondrocyte terminal differentiation [61] and osteogenesis of adipocyte-derived stromal cells in a dose-dependent and irreversible manner [62]. Inclusion of bFGF in culture medium also downregulated the expression of adipogenic genes, thereby inhibiting adipogenesis and lipid accumulation [62-64].

In summary, manipulation of stem cell cultures for propagation, pluripotency maintenance, or differentiation requires specific culture conditions (e.g. substrate surface roughness, stiffness, and degree of hydrophobicity as well as the presence of certain growth factors) [33]. While these 2D and 3D PCL scaffolds did not exhibit a high capacity for stemness maintenance or differentiation induction, they markedly influenced cell growth, survival, and phenotype due to differences in topography and surface hydrophilicity. Two-dimensional scaffolds are suitable for cell propagation and tissue layer preparation whilst 3D scaffolds are widely applied for tissue formation [65]. Plasma oxygen treatment also improves biocompatibility by creating surface properties advantageous for cell–matrix interactions [31]. Hence, PLC scaffolds may offer various options for stem cell fate modulation when combined with certain growth factors and appropriate culture conditions.

5. Conclusions

This study describes the effects of oxygen plasma-treated and untreated 2D and 3D PCL scaffolds on the attachment, proliferation, survival, stemness, and differentiation of hWJMSCs. Both 2D and 3D PCL scaffolds enhanced cell attachment and proliferation compared to a commercial substrate (PS) but slightly altered the stemness properties. These scaffolds also decreased apoptosis and protected cells from death via programmed necrosis. Compared to untreated scaffolds, oxygen plasma-treated scaffolds exhibited greater biocompatibility as manifested by improved cell attachment and proliferation. The 2D platform appeared more suitable for rapid cell adherence and propagation while the 3D scaffolds offered greater opportunity for cell migration. In conclusion, PCL scaffolds exhibit flexible properties that can be manipulated to either enhance or inhibit cell propagation, differentiation, and migration of specific target cells for specific regenerative medicine and tissue engineering applications.

Funding: This research has been partly funded by the Materials Science Research Center (MsRC), Chiang Mai University, Thailand and National Metal and Materials Technology Center, Pathumthani, Thailand (Project code: 2558-00598 FD-StemCells).

Acknowledgments: We would like to thank the Human and Animal Cell Technology Research Unit, Department of Biology, Faculty of Science, Chiang Mai University, Thailand for institutional support. Appreciation from us would be given to all the BSc project students involved in this work.

Conflicts of Interest: The authors declare no conflict of interest.

References

1. Abbasi, N.; Soudi, S.; Hayati-Roodbari, N.; Dodel, M.; Soleimani, M. The effects of plasma treated electrospun nanofibrous poly (ε-caprolactone) Scaffolds with different orientations on mouse embryonic stem cell proliferation. *Cell J.* **2014**, *16*, 245–254.
2. Düzyer, S.; Koral Koç, S.; Hockenberger, A.; Evke, E.; Kahveci, Z.; Uğuz, A. Effects of different sterilization methods on polyester surfaces. *Tekst. ve Konfeksiyon* **2013**, *23*, 319–324, DOI:10.1080/01638538909544723.
3. Augustine, R.; Saha, A.; Jayachandran, V.P.; Thomas, S.; Kalarikkal, N. Dose-dependent effects of gamma irradiation on the materials properties and cell proliferation of electrospun polycaprolactone tissue engineering scaffolds. *Int. J. Polym. Mater. Polym. Biomater.* **2015**, *64*, 526–533, DOI:10.1080/00914037.2014.977900.
4. Zhu, W.; Castro, N.J.; Cheng, X.; Keidar, M.; Zhang, L.G. Cold atmospheric plasma modified electrospun scaffolds with embedded microspheres for improved cartilage regeneration. *PLoS One* **2015**, *10*, e0134729, DOI:10.1371/journal.pone.0134729.
5. Volarevic, V.; Markovic, B.S.; Gazdic, M.; Volarevic, A.; Jovicic, N.; Arsenijevic, N.; Armstrong, L.; Djonov, V.; Lako, M.; Stojkovic, M. Ethical and safety issues of stem cell-based therapy. *Int. J. Med. Sci.* **2018**, *15*, 36–45, DOI:10.7150/ijms.21666.
6. Wu, R.-X.; Xu, X.-Y.; Wang, J.; He, X.-T.; Sun, H.-H.; Chen, F.-M. Biomaterials for endogenous regenerative medicine: Coaxing stem cell homing and beyond. *Appl. Mater. Today* **2018**, *11*, 144–165, DOI:10.1016/J.APMT.2018.02.004.
7. Chen, F.-M.; Wu, L.-A.; Zhang, M.; Zhang, R.; Sun, H.-H. Homing of endogenous stem/progenitor cells for in situ tissue regeneration: Promises, strategies, and translational perspectives. *Biomaterials* **2011**, *32*, 3189–3209, DOI:10.1016/J.BIOMATERIALS.2010.12.032.
8. Pappa, A.M.; Karagkiozaki, V.; Krol, S.; Kassavetis, S.; Konstantinou, D.; Pitsalidis, C.; Tzounis, L.; Pliatsikas, N.; Logothetidis, S. Oxygen-plasma-modified biomimetic nanofibrous scaffolds for enhanced compatibility of cardiovascular implants. *Beilstein J. Nanotechnol.* **2015**, *6*, 254–62, DOI:10.3762/bjnano.6.24.
9. Gilbert, P.M.; Blau, H.M. Engineering a stem cell house into a home. *Stem Cell Res. Ther.* **2011**, *2*, 3, DOI:10.1186/scrt44.
10. Kosorn, W.; Thavornyutikarn, B.; Uppanan, P.; Kaewkong, P. Surface modification of polycaprolactone ccaffolds by plasma treatment for chondrocyte culture. *IPCBEE* **2012**, *43*, 44–48, DOI:10.7763/IPCBEE.
11. Inthanon, K.; Daranarong, D.; Techaikool, P.; Punyodom, W.; Khaniyao, V.; Bernstein, A.M.; Wongkham, W. Biocompatibility assessment of PLCL-sericin copolymer membranes using Wharton's jelly mesenchymal stem cells. *Stem Cells Int.* **2016**, *2016*, DOI:10.1155/2016/5309484.
12. Lim, S.H.; Liu, X.Y.; Song, H.; Yarema, K.J.; Mao, H.-Q. The effect of nanofiber-guided cell alignment on the preferential differentiation of neural stem cells. *Biomaterials* **2010**, *31*, 9031–9039, DOI:10.1016/J.BIOMATERIALS.2010.08.021.
13. Türkoˇ Glu¸sa¸smazelglu¸ Glu¸sa¸glu¸sa¸smazel, H.; Manolache, S.; Menem¸se, M.; Gümü¸sderelioˇ Glu, G. Water/O2-plasma-assisted treatment of PCL membranes for biosignal immobilization. *J. Biomater. Sci.* **2009**, *20*, 1137–1162, DOI:10.1163/156856209X444475.
14. Rampichová, M.; Chvojka, J.; Buzgo, M.; Prosecká, E.; Mikeš, P.; Vysloužilová, L.; Tvrdík, D.; Kochová, P.; Gregor, T.; Lukáš, D.; Amler, E. Elastic three-dimensional poly (ε-caprolactone) nanofibre scaffold enhances migration, proliferation and osteogenic differentiation of mesenchymal stem cells. *Cell Prolif.* **2013**, *46*, 23–37, DOI:10.1111/cpr.12001.
15. Mousavi, S.H.; Abroun, S.; Soleimani, M.; Mowla, S.J. Expansion of human cord blood hematopoietic stem/progenitor cells in three-dimensional nanoscaffold coated with fibronectin. *Int. J. Hematol. stem cell Res.* **2015**, *9*, 72–9.
16. You, R.; Li, X.; Liu, Y.; Liu, G.; Lu, S.; Li, M. Response of filopodia and lamellipodia to surface topography on micropatterned silk fibroin films. *J. Biomed. Mater. Res. Part A* **2014**, *102*, n/a-n/a, DOI:10.1002/jbm.a.35097.
17. Chiarugi, P.; Biochimiche, S. Reactive oxygen species as mediators of cell adhesion. *J. Biochem.* **2003**, *52*, 28–32.
18. Hauck, C.R.; Hsia, D.A.; Schlaepfer, D.D. The focal adhesion kinase--A regulator of cell migration and invasion. *IUBMB Life (International Union Biochem. Mol. Biol. Life)* **2002**, *53*, 115–119, DOI:10.1080/15216540211470.

19. Pirone, D.M.; Liu, W.F.; Ruiz, S.A.; Gao, L.; Raghavan, S.; Lemmon, C.A.; Romer, L.H.; Chen, C.S. An inhibitory role for FAK in regulating proliferation: A link between limited adhesion and RhoA-ROCK signaling. *J. Cell Biol.* **2006**, *174*, 277–288, DOI:10.1083/jcb.200510062.
20. Tomakidi, P.; Schulz, S.; Proksch, S.; Weber, W.; Steinberg, T. Focal adhesion kinase (FAK) perspectives in mechanobiology: implications for cell behaviour. *Cell Tissue Res.* **2014**, *357*, 515–526, DOI:10.1007/s00441-014-1945-2.
21. Gérard, C.; Goldbeter, A. The balance between cell cycle arrest and cell proliferation: control by the extracellular matrix and by contact inhibition. *Interface Focus* **2014**, *4*, 20130075, DOI:10.1098/rsfs.2013.0075.
22. Yam, C.H.; Fung, T.K.; Poon, R.Y.C. Cyclin A in cell cycle control and cancer. *Cell. Mol. Life Sci.* **2002**, *59*, 1317–1326, DOI:10.1007/s00018-002-8510-y.
23. Hochegger, H.; Takeda, S.; Hunt, T. Cyclin-dependent kinases and cell-cycle transitions: does one fit all? *Nat. Rev. Mol. Cell Biol.* **2008**, *9*, 910–916, DOI:10.1038/nrm2510.
24. Sangsanoh, P.; Waleetorncheepsawat, S.; Suwantong, O.; Wutticharoenmongkol, P.; Weeranantanapan, O.; Chuenjitbuntaworn, B.; Cheepsunthorn, P.; Pavasant, P.; Supaphol, P. In vitro biocompatibility of schwann cells on surfaces of biocompatible polymeric electrospun fibrous and solution-cast film scaffolds. *Biomacromolecules* **2007**, *8*, 1587–1594, DOI:10.1021/bm061152a.
25. Teo, B.K.K.; Wong, S.T.; Lim, C.K.; Kung, T.Y.S.; Yap, C.H.; Ramagopal, Y.; Romer, L.H.; Yim, E.K.F. Nanotopography modulates mechanotransduction of stem cells and induces differentiation through focal adhesion kinase. *ACS Nano* **2013**, *7*, 4785–4798, DOI:10.1021/nn304966z.
26. Yang, S.-T.; Ng, R. A new dimension to biomaterials. *Mater. Today* **2007**, *10*, 64, DOI:10.1016/S1369-7021(07)70030-5.
27. Provenzano, P.P.; Keely, P.J. Mechanical signaling through the cytoskeleton regulates cell proliferation by coordinated focal adhesion and Rho GTPase signaling. *J. Cell Sci.* **2011**, *124*, 1195–1205, DOI:10.1242/jcs.067009.
28. Vishnubhotla, R.; Bharadwaj, S.; Sun, S.; Metlushko, V.; Glover, S.C. Treatment with Y-27632, a ROCK inhibitor, increases the proinvasive nature of SW620 cells on 3d collagen type 1 matrix. *Int. J. Cell Biol.* **2012**, *2012*, DOI:10.1155/2012/259142.
29. Wu, S.; Liu, X.; Yeung, A.; Yeung, K.W.K.; Kao, R.Y.T.; Wu, G.; Hu, T.; Xu, Z.; Chu, P.K. Plasma-modified biomaterials for self-Antimicrobial applications. *ACS Appl. Mater. Interfaces* **2011**, *3*, 2851–2860, DOI:10.1021/am2003944.
30. Kumari, T.V.; Vasudev, U.; Kumar, A.; Menon, B. Cell surface interactions in the study of biocompatibility. *Trends Biomater. Artif. Organs* **2001**, *15*, 37–41.
31. Michaelis, S.; Robelek, R.; Wegener, J. Studying cell-surface interactions in vitro: a survey of experimental approaches and techniques. *Adv. Biochem. Engin./Biotechnol.* **2012**, *126*, 33–66, DOI: 10.1007/10_2011_112.
32. Chen, F.-M.; Wu, L.-A.; Zhang, M.; Zhang, R.; Sun, H.-H. Homing of endogenous stem/progenitor cells for in situ tissue regeneration: Promises, strategies, and translational perspectives. *Biomaterials* **2011**, *32*, 3189–3209, DOI:10.1016/J.BIOMATERIALS.2010.12.032.
33. You, R.; Li, X.; Liu, Y.; Liu, G.; Lu, S.; Li, M. Response of filopodia and lamellipodia to surface topography on micropatterned silk fibroin films. *J. Biomed. Mater. Res. Part A* **2014**, *102*, n/a-n/a, DOI:10.1002/jbm.a.35097.
34. Collart-Dutilleul, P.-Y.; Panayotov, I.; Secret, E.; Cunin, F.; Gergely, C.; Cuisinier, F.; Martin, M. Initial stem cell adhesion on porous silicon surface: molecular architecture of actin cytoskeleton and filopodial growth. *Nanoscale Res. Lett.* **2014**, *9*, 564, DOI:10.1186/1556-276X-9-564.
35. Inthanon, K.; Saranwong, N.; Wongkham, W.; Wanichapichart, P.; Prakrajang, K.; Suwannakachorn, D.; Yu, L.D. PIII-induced enhancement and inhibition of human cell attachment on chitosan membranes. *Surf. Coatings Technol.* **2013**, *229*, 112–119, DOI:10.1016/J.SURFCOAT.2012.10.042.
36. Vignesh; Nayar, S.; Bhuminathan; Mahadevan; Santhosh, S. Comparative evaluation of the three different surface treatments - conventional, laser and nano technology methods in enhancing the surface characteristics of commercially pure titanium discs and their effects on cell adhesion: An in vitro study. *J. Pharm. Bioallied Sci.* **2015**, *7*, S87-91, DOI:10.4103/0975-7406.155817.
37. Thies, E.; Davenport, R.W. Independent roles of Rho-GTPases in growth cone and axonal behavior. *J Neurobiol* **2003**, *54*, 358–369, DOI:10.1002/neu.10135.

38. Bergert, M.; Chandradoss, S.D.; Desai, R.A.; Paluch, E. Cell mechanics control rapid transitions between blebs and lamellipodia during migration. *Proc. Natl. Acad. Sci. U. S. A.* **2012**, *109*, 14434–9, DOI:10.1073/pnas.1207968109.
39. Albuschies, J.; Vogel, V. The role of filopodia in the recognition of nanotopographies. *Sci. Rep.* **2013**, *3*, 1658, DOI:10.1038/srep01658.
40. Dalby, M.J.; Gadegaard, N.; Tare, R.; Andar, A.; Riehle, M.O.; Herzyk, P.; Wilkinson, C.D.W.; Oreffo, R.O.C. The control of human mesenchymal cell differentiation using nanoscale symmetry and disorder. *Nat. Mater.* **2007**, *6*, 997–1003, DOI:10.1038/nmat2013.
41. Fletcher, D.A.; Mullins, R.D. Cell mechanics and the cytoskeleton. *Nature* **2010**, *463*, 485–92, DOI:10.1038/nature08908.
42. Milner, K.R.; Siedlecki, C.A. Fibroblast response is enhanced by poly(L-lactic acid) nanotopography edge density and proximity. *Int. J. Nanomedicine* **2007**, *2*, 201–11.
43. Wang, K.; Bruce, A.; Mezan, R.; Kadiyala, A.; Wang, L.; Dawson, J.; Rojanasakul, Y.; Yang, Y. Nanotopographical modulation of cell function through nuclear deformation. *ACS Appl. Mater. Interfaces* **2016**, *8*, 5082–5092, DOI:10.1021/acsami.5b10531.
44. Hsuuw, Y.; Chan, W. Dose-Dependently Induces Apoptosis or Necrosis in Human MCF-7 Cells. *New York* **2007**, *440*, 428–440, DOI:10.1196/annals.1397.046.
45. Edinger, A.L.; Thompson, C.B. Death by design: apoptosis, necrosis and autophagy. *Curr. Opin. Cell Biol.* **2004**, *16*, 663–669, DOI:10.1016/J.CEB.2004.09.011.
46. McIlwain, D.R.; Berger, T.; Mak, T.W. Caspase functions in cell death and disease. *Cold Spring Harb. Perspect. Biol.* **2013**, *5*, 1–28, DOI:10.1101/cshperspect.a008656.
47. Bitzer, M.; Armeanu, S.; Prinz, F.; Ungerechts, G.; Wybranietz, W.; Spiegel, M.; Bernlöhr, C.; Cecconi, F.; Gregor, M.; Neubert, W.J.; Schulze-Osthoff, K.; Lauer, U.M. Caspase-8 and Apaf-1-independent caspase-9 activation in Sendai virus-infected cells. *J. Biol. Chem.* **2002**, *277*, 29817–29824, DOI:10.1074/jbc.M111898200.
48. Stegh, A.H.; Barnhart, B.C.; Volkland, J.; Algeciras-Schimnich, A.; Ke, N.; Reed, J.C.; Peter, M.E. Inactivation of caspase-8 on mitochondria of Bcl-xL-expressing MCF7-Fas cells: role for the bifunctional apoptosis regulator protein. *J. Biol. Chem.* **2002**, *277*, 4351–60, DOI:10.1074/jbc.M108947200.
49. Sosna, J.; Voigt, S.; Mathieu, S.; Lange, A.; Thon, L.; Davarnia, P.; Herdegen, T.; Linkermann, A.; Rittger, A.; Chan, F.K.-M.; Kabelitz, D.; Schütze, S.; Adam, D. TNF-induced necroptosis and PARP-1-mediated necrosis represent distinct routes to programmed necrotic cell death. *Cell. Mol. Life Sci.* **2014**, *71*, 331–348, DOI:10.1007/s00018-013-1381-6.
50. Kracikova, M.; Akiri, G.; George, A.; Sachidanandam, R.; Aaronson, S.A. A threshold mechanism mediates p53 cell fate decision between growth arrest and apoptosis. *Cell Death Differ.* **2013**, *20*, 576–88, DOI:10.1038/cdd.2012.155.
51. Chipuk, J.E.; Fisher, J.C.; Dillon, C.P.; Kriwacki, R.W.; Kuwana, T.; Green, D.R. Mechanism of apoptosis induction by inhibition of the anti-apoptotic BCL-2 proteins. *Proc. Natl. Acad. Sci. U. S. A.* **2008**, *105*(*51*), 20327–20332. DOI:10.1073/pnas.0808036105.
52. Buxton, A.N.; Zhu, J.; Marchant, R.; West, J.L.; Yoo, J.U.; Johnstone, B. Design and characterization of poly(ethylene glycol) photopolymerizable semi-interpenetrating networks for chondrogenesis of human mesenchymal stem cells. *Tissue Eng.* **2007**, *13*, 2549–2560, DOI:10.1089/ten.2007.0075.
53. Chan, B.P.; Hui, T.Y.; Yeung, C.W.; Li, J.; Mo, I.; Chan, G.C.F. Self-assembled collagen–human mesenchymal stem cell microspheres for regenerative medicine. *Biomaterials* **2007**, *28*, 4652–4666, DOI:10.1016/J.BIOMATERIALS.2007.07.041.
54. Hofmann, S.; Hagenmüller, H.; Koch, A.M.; Müller, R.; Vunjak-Novakovic, G.; Kaplan, D.L.; Merkle, H.P.; Meinel, L. Control of in vitro tissue-engineered bone-like structures using human mesenchymal stem cells and porous silk scaffolds. *Biomaterials* **2007**, *28*, 1152–1162, DOI:10.1016/J.BIOMATERIALS.2006.10.019.
55. Noisa, P.; Ramasamy, T.S.; Lamont, F.R.; Yu, J.S.L.; Sheldon, M.J.; Russell, A.; Jin, X.; Cui, W. Identification and characterisation of the early differentiating cells in neural differentiation of human embryonic stem cells. *PLoS One* **2012**, *7*, e37129, DOI:10.1371/journal.pone.0037129.
56. Weiss, M..; Mitchell, K..; Hix, J..; Medicetty, S.; El-Zarkouny, S..; Grieger, D.; Troyer, D.. Transplantation of porcine umbilical cord matrix cells into the rat brain. *Exp. Neurol.* **2003**, *182*, 288–299, DOI:10.1016/S0014-4886(03)00128-6.

57. Qian, J.; Habegger, L.; Noisa, P.; Szekely, A.; Qiu, C.; Hutchison, S.; Raha, D. Dynamic transcriptomes during neural differentiation of human embryonic stem cells revealed by short , long , and paired-end sequencing. **2010**, *107*, DOI:10.1073/pnas.0914114107.
58. Gharibi, B.; Hughes, F.J. Effects of medium supplements on proliferation, differentiation potential, and in vitro expansion of mesenchymal stem cells. *Stem Cells Transl. Med.* **2012**, *1*, 771–782, DOI:10.5966/sctm.2010-0031.
59. Wolfe, M.; Tucker, A.; Reger, R.L.; Prockop, D.J. Multipotent Stromal Cells (hMSCs). In *Human Adult Stem Cells*; Masters, J.R., Palsson, B.Ø., Eds.; Springer Netherlands: Dordrecht, 2009; pp. 45–72 ISBN 978-90-481-2269-1.
60. Lawrence, B.J.; Madihally, S. V. Cell colonization in degradable 3D porous matrices. *Cell Adh. Migr.* **2008**, *2*, 9–16, DOI:10.4161/cam.2.1.5884.
61. Grigore, M.E. Biomaterials for cartilage tissue engineering. *J. Tissue Sci. Eng.* **2017**, *08*, 4–9, DOI:10.4172/2157-7552.1000192.
62. Quarto, N.; Longaker, M.T. FGF-2 Inhibits osteogenesis in mouse adipose tissue-derived stromal cells and sustains their proliferative and osteogenic potential state. *Tissue Eng.* **2006**, *12*, 1405–1418, DOI:10.1089/ten.2006.12.1405.
63. Webb, P.R.; Doyle, C.; Anderson, N.G. Protein kinase C-ε promotes adipogenic commitment and is essential for terminal differentiation of 3T3-F442A preadipocytes. *Cell. Mol. Life Sci.* **2003**, *60*, 1504–1512, DOI:10.1007/s00018-003-2337-z.
64. Miyaoka, Y.; Tanaka, M.; Naiki, T.; Chemistry, A.M.-J. of B. Oncostatin M inhibits adipogenesis through the RAS/ERK and STAT5 signaling pathways. *J. Biol. Chem.* **2006**, *281*(49), 37913–37920, DOI:10.1074/jbc.m606089200.
65. Zhang, Z.; Gupte, M.J.; Ma, P.X. Biomaterials and stem cells for tissue engineering. *Expert Opin. Biol. Ther.* **2013**, *13*, 527–40, DOI:10.1517/14712598.2013.756468.